Journal of Polymer Research (2025) 32:242
https://doi.org/10.1007/s10965-025-04466-1

ORIGINAL PAPER

Preparation of hydrogel adsorbents with functional sulfone groups for removal of cationic dyes from aqueous solution

Gulay Bayramoglu[1,2] · Murat Kılıc[1] · Ilkay Acıkgoz-Erkaya[3] · Orhan Hazer[4] · Mehmet Yakup Arica[1]

Received: 14 February 2025 / Accepted: 18 June 2025 / Published online: 3 July 2025
© The Polymer Society, Taipei 2025

Abstract

In this study, sulfone groups carrying a hybrid hydrogel were synthesized through network-forming redox polymerization in the presence of a redox initiator pair. Through the defined one-pot polymer synthesis chemistry, the hybrid hydrogel with 2-acrylamido-2-methyl-1-propanesulfonic acid (APSA) and 2-hydroxyethylmethacrylate (HEMA) with its well-known advantages and high affinity toward cationic micro-pollutants by ion-exchange route had been synthesized. The prepared hydrogels were characterized using ATR-FTIR spectroscopy, SEM, zeta-sizer, swelling studies, and the BET method. The dye adsorption performance of the hydrogel adsorbent was determined with cationic dyes, Crystal Violet (CV), and a carcinogen dye, Congo Red (CR). The effect of various system parameters, such as contact time, adsorbent dose, ionic strength, medium pH, initial dye concentration, and temperature, was tested for the adsorption of CV and CR dyes in the hydrogels. The maximum adsorption capacity for the p(HEMA-APSA)-2 hydrogel at 25 °C was 306.1 and 186.9 mg/g for CV and CR, respectively. The Langmuir isotherm model is more suitable for fitting the experimental data for CV and CR adsorption. The adsorption capacity of p(HEMA-APSA)-2 hydrogel for CV and CR dyes increased by 2.1 and 2.3 fold, respectively, by increasing the temperature from 15 °C to 45 °C. CV and CR adsorption were spontaneous and endothermic based on thermodynamic studies. After five repeated use cycles, p(HEMA-APSA)-2 hydrogel could be repeatedly used with high stability. A comprehensive investigation of the hydrogel adsorbent showed that it has promising potential for removing pollutants from solution.

Keywords Hydrogel · Adsorption · Cationic dye · Isotherms and kinetic studies

Introduction

Wastewater treatment has become one of the major research areas emerging due to increasing population rate, domestic wastewater generation, rapid industrialization, climate change, pesticide use in agriculture, and environmental changes [1–3]. The ongoing release of pollutants into natural water bodies leads to serious problems for living systems [4–6]. Different organic pollutants such as textile dyes, drugs, pesticides, and cosmetics have been detected in aquatic environments [7–10]. Among these organic pollutants, textile dyes have more detrimental results on aquatic systems due to their longer half-life and low biodegradability. Textile industries produce large amounts of dye waste due to the high amount of water used in dyeing processes. The widespread use of these dyes in various industries such as textiles, leather, cosmetics, pharmaceuticals, plastics, and food has increased the severity of water pollution. Moreover, even minimal amounts of dye in water (less than 1.0 ppm for some dyes) are apparent and undesirable because they prevent light penetration into water and generate ecotoxicological effects on aquatic plants and organisms [11–15]. Approximately 100000 various dyes and pigments are

✉ Gulay Bayramoglu
g_bayramoglu@hotmail.com

1 Biochemical Processing and Biomaterial Research Laboratory, Gazi University, Teknikokullar, Ankara 06500, Turkey

2 Department of Chemistry, Faculty of Sciences, Gazi University, Teknikokullar, Ankara 06500, Turkey

3 Department of Environmental Science, Faculty of Engineering and Architecture, Ahi Evran University, Kırsehir 40100, Turkey

4 Department of Chemistry, Faculty of Sciences, Yozgat Bozok University, Yozgat 66900, Turkey

produced worldwide, and the amount of dye production is higher than 7×10^5 tons per year. Therefore, dyes must be reduced from industrial wastewater to an acceptable level before being released into the environment. Moreover, these dyes are toxic, carcinogenic, and mutagenic, and their complex aromatic structure makes them stable and difficult to remove from wastewater [15–19]. Consequently, eliminating these dyes from wastewater is important, and a useful removal method is necessary for environmental sustainability [20, 21]. Numerous water treatment methods have been described for removing organic pollutants from wastewater, such as adsorption, biosorption, photocatalytic degradation, membrane separation, precipitation, and biodegradation [17, 22–27]. Among these methods, adsorption is a suitable approach due to its facile and low operation cost, low energy requirement, good removal efficacy, high adsorption capacity, ease of adaptation to large-scale operation, and no byproduct formation during adsorption. The hydrogel based adsorbents have been prepared from various hydrophilic monomers with the desired functional group density, high surface area, and good porosity [28]– [29]. Hydrogel based adsorbents exhibit an effective adsorption achievement due to their three-dimensional network of polymer chains and hydrophilic nature of polymers [29, 30]. Moreover, hydrogel adsorbents are inexpensive, non-toxic, and stable to against many chemical and biological reactions, and also they have good reusability [19, 20]. Furthermore, hydrogels based adsorbents show high adsorption performance to remove various inorganic and organic pollutants from aqueous media even at their lower concentrations, whichever can make them useful for extensive use in environmental applications [24, 25, 31]. Synthetic and natural hydrogels such as chitin, chitosan, alginate, cellulose, cellulose derivative, acrylic polymers and silica gels have been used as adsorbent to remove pollutants from wastewaters [31–36]. The hydrogel adsorbents can be easily prepared using functional monomers, with high surface area, good porosity, and high chemical stability. The available groups on the hydrogel adsorbents, such as aromatic, amine, carboxyl, phosphate, hydroxyl, and sulfone, can associate via noncovalent interactions with the functional groups of target pollutants. Thus, these hydrogel adsorbents can be efficiently used for removal of textile dyes, phenols, pesticides, and pharmaceuticals [31–41]. For examples, a hydrogel network was prepared from pullulan, polydopamine and 1–6-Hexanediol diglycidyl ether via the chemical cross-linking method and, the adsorption capacity of the hydrogel was 107 mg/g toward Crystal violet [31]. Kappa-carrageenan was grafted by acrylamide and maleic acid monomers in the presence of multi-walled carbon nanotubes by using N, N'-methylene bisacrylamide crosslinker.The maximum adsorption capacity of the hydrogel for crytal violet dye was 84 mg/g [32]. A biocomposite hydrogel was synthesized from pine needles with chitosan and gelatin. The biocomposite hydrogel was used for the removal of cationic dyes (i.e., Malachite green, Methylene blue, and Crystal violet and anionic dyes (i.e., Methyl orange and Congo red), and the maximum adsorption capacity of the biocomposite for the mixture of dyes was 307.9 mg/g [33]. A MXene composited hydrogel was prepared from cysteine-grafted hydroxyethyl methacrylate, exhibiting high selectivity toward ionic dyes at different pH. The adsorption capacity of PHGC/MXene hydrogel for Methylene blue and Methyl blue was reported as 207.5 and 555.6 mg/g, respectively [34]. Amine groups and copper ions incorporated particles were embedded in poly (2-hydroxyethyl methacrylate) hydrogels, and the adsorption capacity of the as prepared adsorbent was 816.0 and 648.0 mg/g toward Reactive green 19 dye, respectively [35]. Gellan gum based hydrogel was synthesized via esterification of gellan gum with maleic anhydride and cross-linking via thiol − ene chemistry and the adsorption capacity of was found to be 547 mg/g toward Methylene blue [36]. Hydrogel adsorbents have been prepared from synthetic and natural materials and heavily utilized in wastewater treatment. However, there is still a need for new research in this field to synthesize hydrogels with high adsorption capacity and easy to prepare.

This study aims to synthesize a series of hydrogel adsorbents with desired functional sulfone group density with high removal efficiency toward two cationic dyes, CV and CR, from aqueous media. The novelty of the present work is based on the synthesis of hydrogel adsorbents with desired adsorption capacity and mechanical strength by adding various amounts of functional monomer (i.e., APSA) to the polymerization mixtures for the removal of cationic (i.e., CV and CR) dyes. In this direction, the hydrogels containing different amounts of the sulfone groups using APSA monomer were prepared using the one-pot method. 2-hydroxyethyl methacrylate and 2-Acrylamido-2-methylpropane sulfonic acid are hydrophilic monomers; the protonation–deprotonation properties of the sulfonic acid groups of the latter monomer ($-SO_3H$) can provide binding sites for the adsorption of a variety of pollutants, including hazardous non-biodegradable dyes. Also, the ratio of the second monomer can control the swelling ratio and elasticity of the as-prepared adsorbents. Further, the technique can be effective because the adsorptive groups can be easily incorporated into the hydrogel adsorbent at a desired density by adjusting the concentration of functional groups

carrying co-monomer in the polymerization mixture. The hydrogel adsorbent was characterized using FTIR, SEM, zeta-potential, BET method, and swelling studies. The efficiency of p(HEMA-APSA)−1-3 removing CV and CR was carefully evaluated using p(HEMA) as a control system through detailed batch adsorption studies. The effect of sulfone group density in the gel structure on the adsorption performance was also evaluated to determine the optimum amount of sulfone group density. The effects of various parameters such as contact time, adsorbent dose, medium pH, ionic strength, initial dye concentration, and temperature on the removal of both tested dyes were studied using p(HEMA-APSA)−2. Reusability studies of the p(HEMA-APSA)−2 hydrogel using NaOH solution were realized. Furthermore, experimental data were analyzed using adsorption isotherms and kinetics models to assess the effect of polyanionic groups of the adsorbents during interaction with CV and CR dyes. The adsorption mechanism of both dyes on the adsorbent and the effect of functional group densities on the adsorption capacities of dyes were evaluated.

Materials and methods

Materials

Crystal Violet ($C_{25}H_{30}N_3Cl$; MW: 407.98; λ_{max}: 590 nm) and Congo Red ($C_{32}H_{22}N_6Na_2O_6S_2$; MW: 696.66; λ_{max}: 498 nm) dyes were obtained from Sigma-Aldrich (St. Louis, MO, USA). The properties of the CV and CR dyes are presented in Table 1. 2-Hydroxyethyl methacrylate (HEMA) and 2-acrylamido-2-methyl-1-propanesulfonic acid (APSA) were obtained from Sigma-Aldrich. N, N'-Methylenebis(acrylamide) (BAAm) was obtained from Fluka A.G., Buchs, Switzerland. Sodium chloride and isopropyl alcohol (2-propanol) were obtained from Merck A.G. (Darmstadt, Germany). Polyvinyl alcohol (PVA), ammonium persulfate (APS), and N, N, N', N'-tetramethylenediamine (TEMED) were supplied from Sigma-Aldrich.

Synthesis of the p(HEMA-APSA) hydrogel formulations

Hydrogels carrying functional sulfone (i.e., $-SO_3H$) groups were synthesized using the HEMA and APSA monomers in the presence of N, N' methylene-bis(acrylamide) as a cross-linker. In the polymerization mixture, the amount of APSA was varied. Polymerization reaction was initiated using ammonium persulfate (APS) and tetramethylenediamine (TEMED) redox polymerization initiator pairs at room temperature. Polymer formulations were prepared by completing to 6.0 mL with distilled water the volume of the polymerization mixture containing a fixed amount of HEMA (2.0 mL) and N, N'-methylene-bis(acrylamide) (54 mg) and varying amounts of functional APSA monomer (0.25, 0.50, or 1.00 g). APS (50 µL) and TEMED (50 µL, 10%) were added to this solution as an initiator and activator, respectively, and nitrogen gas was passed for 2.0 min. It was transferred to a cylinder glass column (diameter 1.0 cm), sealed with parafilm and a plastic stopper, and allowed to react for 1.0 h at room temperature. The synthesized hydrogels were washed with distilled water and dried at 40 °C in a vacuum. They were sieved by molecular sieve, and the size distribution was determined. The as-prepared hydrogel adsorbents were called the p(HEMA-APSA)−1, p(HEMA-APSA)−2, and p(HEMA-APSA)−3.

Table 1 Properties of congo red and crystal Violet dyes

	Congo Red	Crystal Violet
Synonym of dye	Direct Red 128	Brilliant Violet
H-bond donors	2	0
H-bond acceptors	12	3
EC number	209–358–4	548-62-9
Color index number	22120	42555
Chemical formula	$C_{32}H_{22}N_6Na_2O_6S_2$	$C_{25}H_{30}ClN_3$
Molar mass	696.71	407.98
λ_{max} (nm)	495	590
Chemical structure	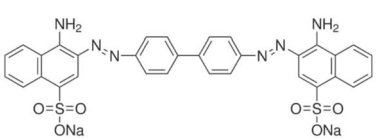	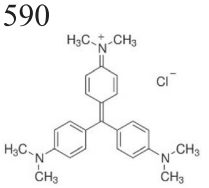

Characterization studies

The surface morphology of the p(HEMA) and p(HEMA-APSA)−3 hydrogel particles was determined by scanning electron microscopy. The dried samples were coated with a thin layer of gold under reduced pressure, and SEM pictures were obtained using a JEOL JSM 5600 Scanning Electron Microscope, Japan. The BET method (Brunauer, Emmett, and Teller) was used to determine the surface area of the hydrogel particles using a BET device (Quantachrome Nova 2200E, USA).

ATR-FTIR measurements of p(HEMA) and p(HEMA-APSA)−3 hydrogels were made in a Spectrum 100 FTIR spectrometer (Perkin-Elmer Inc., Norwalk, CT, USA) equipped with the ATR accessory. The samples were scanned between 4000 and 525 cm^{-1}. Before the ATR-FTIR measurements, the samples were dried overnight at 40 °C in a vacuum oven.

The equilibrium water content of p(HEMA) and p(HEMA-APSA)−1-3 was determined in distilled water using the gravimetric method. Approximately 1.0 g of hydrogel was placed in a volumetric cylinder containing distilled water and placed in an isothermal water bath at constant temperature (25 ± 0.5 °C), and the equilibrium water content after 24 h was determined. The swelling ratio of the hydrogel was calculated using the following equation:

$$\text{Swelling content } (\%) = [W_s - W_d/W_d]x100 \quad (1)$$

where W_s and W_d are the weights of swollen and dry hydrogel, respectively.

As described previously, the number of sulfone groups of p(HEMA-APSA)−1-3 hydrogels was determined [30]. 0.1 g of hydrogel sample was transferred into NaOH solution (0.1 M, 20 mL) and incubated for 6.0 h at 25 °C while stirring. Then, the sample was titrated with HCl solution (0.05 M).

The mechanical strength of the p(HEMA) and p(HEMA-APSA)−1-3 formulations was studied via elongation experiments. Mechanical strength of p(HEMA), and p(HEMA-APSA)−1, p(HEMA-APSA)−2, and p(HEMA-APSA)−3 were determined from dog-bone shapes (20-mm span length, 3-mm width, and 0.6-mm thickness) cut from the film form samples. The tensile strength and breaking elongation were measured using a mechanical testing machine at room temperature (Lloyd, LS 500, Fareham, Hampshire, England). The software automatically recorded the curve of force as a function of deformation (mm). The tensile modulus (kPa) and elongation at break were calculated at an extension rate of 2 mm/min ($n = 4$).

Zeta potentials of p(HEMA) and p(HEMA-APSA)−2 hydrogels were obtained at various pH values. In a typical experiment, hydrogel particles (0.2 g) were added to a bottle containing distilled water (100 mL), and the mixture was magnetically stirred for about 1.0 h. The desired pH was adjusted, and then used to measure zeta potential value with a Zeta-sizer (NanoZS, Malvern Instruments Ltd., Malvern, UK).

Adsorption studies

The adsorption of CV and CR dyes on p(HEMA-APSA)−1-3 hydrogels was studied in a batch system using p(HEMA) hydrogel particles as a control. The standard CV or CR dye solutions were prepared from the stock solutions containing 500 mg/L dye. The adsorption experiments were investigated at different initial CV and CR dye concentrations (10–200 mg/L). The adsorption studies various adsorbent dosages (0.1 and 1.0 g/L), different ionic strength (0.0–1.0 M NaCl), by changing initial pH (2.0–9.0) and at four different temperatures (15, 25, 35 and 45 °C) were realized and the amount of adsorbed dyes was measured using a double-beam UV-vis spectrophotometer (Model T80+; PG Instrument Ltd., UK). The concentration of CV and CR dyes was measured at their maximum absorption wavelength, 590 and 498 nm, respectively. The amount of adsorbed dye on the p(HEMA) and p(HEMA-APSA)−1-3 hydrogels was calculated using the following equation:

$$q = (C_0 - C)V/m \quad (2)$$

where C_0 and C are the dye concentrations in solution before and after adsorption (mg/L), respectively; q is the amount of dye adsorbed per unit dry mass of the hydrogel (mg/g); V is the dye solution (L) and m is the weight of the dry hydrogel (g). All experiments were repeated three times, and the averages were taken. The adsorption data were evaluated using different theoretical isotherm models, such as the Langmuir and the Freundlich. Finally, the thermodynamic parameters of the adsorption were determined.

Desorption and reusability studies

Five consecutive adsorption/desorption cycles were performed to examine the reusability of p(HEMA-APSA)−1-3 hydrogel particles. The initial concentration of CV and CR dyes was 100 mg/L at 25 °C for 120 min. Then, the CV and CR loaded p(HEMA-APSA)1–3 hydrogel particles were separated from the medium and desorbed with 0.1 mol/L NaOH.

The percentage of dye removal by hydrogel particles was calculated using the following equation:

$$\text{Percentage of Dye Removal } (\%) = [(C_0 - C)/C_0]x100 \quad (3)$$

Results and discussions

Properties of p(HEMA and p(HEMA-APSA)−1-3

One-pot synthesis method was used to prepare p(HEMA) and p(HEMA-APSA)−1-3 hydrogels. The synthesis of hydrogels was realized via redox polymerization route in the presence of APS and TEMED as the initiator and activator, respectively. The schematic representation of the preparation of hydrogels is presented in Fig. 1. To obtain a high adsorption performance towards cationic dye molecules CV and CR dyes, the APSA ratio was varied in the polymerization medium, and the polymerization reaction was completed within 1.0 h. The amount of APSA in the hydrogels was determined via potentiometric titration. The sulfone group content of the p(HEMA-APSA)−1, p(HEMA-APSA)−2, and p(HEMA-APSA)−3 formulations was found to be 0.068, 1.23, and 1.94 mmol/g hydrogels, respectively.

The equilibrium water content of the p(HEMA) hydrogel was determined to be 136.3%. In this polymer structure, each repeating unit has a pendant hydroxyl group, causing hydrophilic properties to the polymer that can be utilized to form a hydrogel. The p(HEMA) hydrogel has better mechanical properties than natural hydrogels and good biological stability. Therefore, p(HEMA) based hydrogels have been used in various biomedical and biotechnological applications such as contact lenses, drug delivery systems, enzyme technology, and wound dressing. The incorporation of APSA monomer in the p(HEMA) structure caused a substantial increase in the water content of the p(HEMA-APSA)−1-3 formulations, about 382.4, 751.9, and 1004.2,

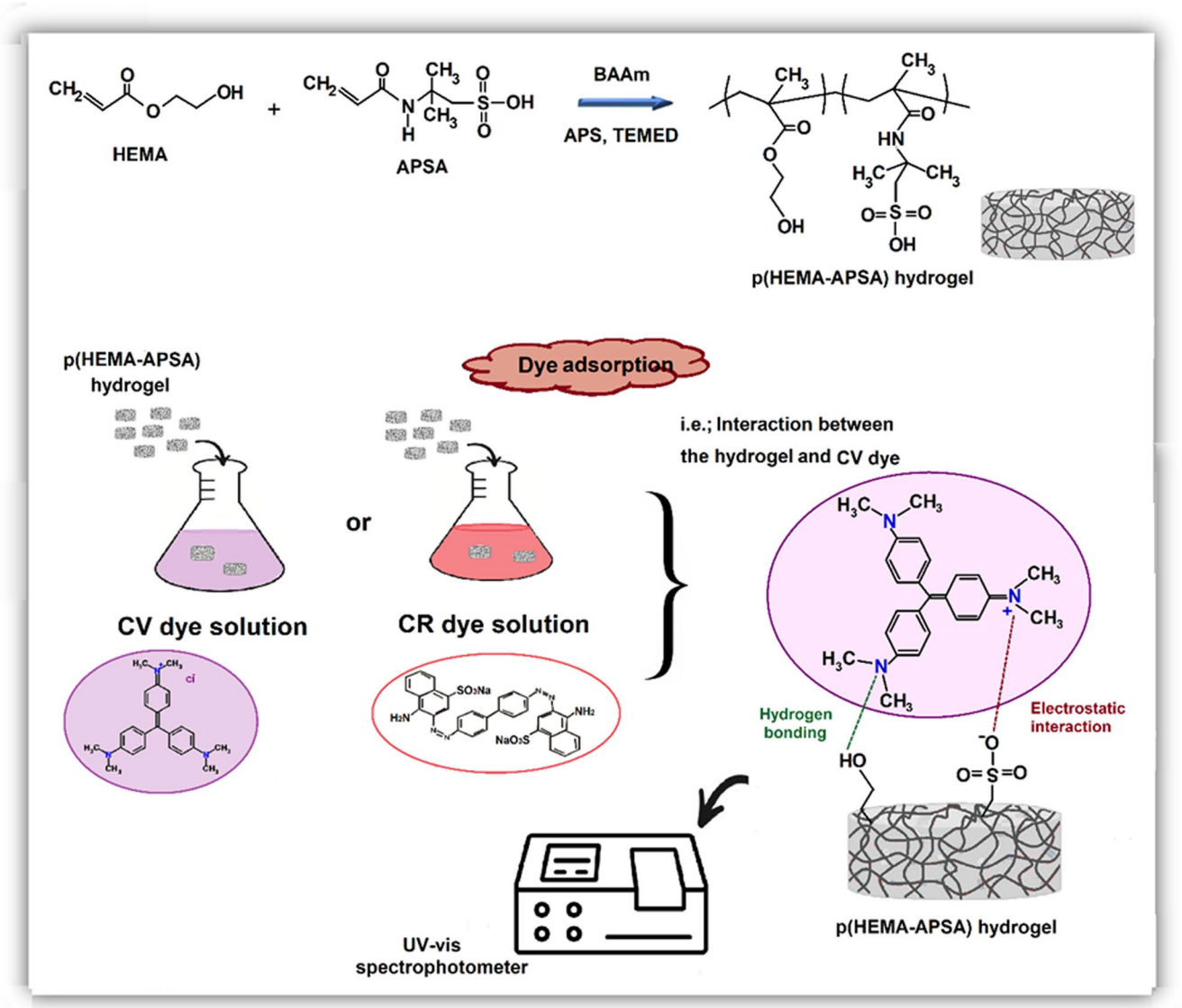

Fig. 1 Schematic representation of experimental protocols

respectively. The equilibrium water content of the p(HEMA-APSA)−3 hydrogel in distilled water was increased by about 7.4-fold. Including the APSA monomer with sulfone groups in the p(HEMA) hydrogel, the equilibrium water content increased approximately 7.4 times for p(HEMA-APSA)−1. The pendant sulfone groups in the AMPSA unit of the copolymer structure resulted in a negative charge on the polymer backbone, leading to its ability to absorb a higher amount of water. The amount of sulfone group contents in the p(HEMA-APSA)−1, p(HEMA-APSA)−2, and p(HEMA-APSA)−3 hydrogels increased as the amount of APSA monomer in the formulations increased, and the water content of the hydrogels was also increased according to APSA content.

The ATR-FTIR spectra of p(HEMA), p(HEMA-APSA)−2, p(HEMA-APSA)−2-CV, and p(HEMA-APSA)−2-CR are presented in Fig. 2. The FTIR spectrum of p(HEMA) hydrogel showed a broad band at around 3370 cm^{-1} due to stretching vibrations of -OH groups. The peaks at 2945 cm^{-1} and 1722 cm^{-1} could be caused by the methylene group's vibrations and ester configuration of HEMA polymer, respectively (Fig. 2A). Whereas, in the FTIR spectrum of p(HEMA-APSA)−2 hydrogels, the wide band in the range 3600–3000 cm^{-1} in the spectrum of the co-polymer could be assigned to the stretching of O–H and N–H bonds (Fig. 2B). The bands at 1649 cm^{-1} and 1549 cm^{-1} could be due to the C—O stretching vibration of the amide I group and the N–H bending of amide II, respectively. The bands observed at 1030 and 1068 cm^{-1} could be attributed to the symmetric and asymmetric stretches of the sulfone groups, respectively. The other important peak observed at 1391 cm^{-1} could be assigned to S=O stretching vibration groups of the APSA unit of the copolymer. After adsorption of CV, a specific peak for benzene rings was observed at 1568 cm^{-1}, which matches the C=C stretching of the benzene ring. The peaks at 1178 cm^{-1} and 2933 cm^{-1} corresponding to the C–N stretching vibrations and C–H stretching of the asymmetric CH_3 group were observed. The broad peak observed at around 2300 cm^{-1} and 1360 cm^{-1} corresponds to a symmetric and asymmetric stretching of tertiary amine groups (Fig. 2C). The p(HEMA-APSA)−2-CR was used to confirm the functional groups of the adsorbed dye. As shown in Fig. 2D, the stretching vibration band of the azo group (-N=N-) from 1504 to 1555 cm^{-1} was seen in the infrared spectrum of Congo red. The 1612 cm^{-1} and 1531 cm^{-1} peaks were typical for the red azo dyes. The stretching vibration of the S=O group appeared at 1190 cm^{-1} and 1341 cm^{-1}.

The equilibrium water content of the p(HEMA) hydrogel was determined to be 136.3%. In this polymer structure, each repeating unit has a pendant hydroxyl group, causing hydrophilic properties to the polymer that can be utilized to form a hydrogel. The p(HEMA) hydrogel has better mechanical properties than natural hydrogels and good biological stability. Therefore, p(HEMA) based hydrogels have been used in various biomedical and biotechnological applications such as contact lenses, drug delivery systems, enzyme technology, and wound dressing. The incorporation of APSA monomer in the p(HEMA) structure caused a substantial increase in the water content of the p(HEMA-APSA)−1-3 formulations. The equilibrium water content of the p(HEMA-APSA)−3 hydrogel in distilled water was increased by about 7.4-fold. Including the APSA monomer with sulfone groups in the p(HEMA) hydrogel, the equilibrium water content increased approximately 7.4 times for p(HEMA-APSA)−1. The pendant sulfone groups in the AMPSA unit of the copolymer structure resulted in a negative charge on the polymer backbone, leading to its ability to absorb a higher amount of water. The amount of sulfone group contents in the p(HEMA-APSA)−1, p(HEMA-APSA)−2, and p(HEMA-APSA)−3 hydrogels increased as the amount of APSA monomer in the formulations increased, and the water content of the hydrogels was also increased according to APSA content (Table 3).

The zeta potential values of p(HEMA) and p(HEMA-APSA)−2 hydrogels were determined at different pH values between 2.0 and 11.0. When particles are dispersed in a liquid, an electrical double layer is frequently generated; this could be due to the particle surfaces mostly having a surface charge that could be attractive to these ions. When the particles change their position, the electrical double layer also changes its position within the liquid, and is called the slipping plane. The electric potential at this slipping plane is referred to as zeta potential. When particles have strong positive or negative zeta potential values, there is also a strong repulsive electrostatic interaction between the particles, which prevents the particles from approaching each other and forming clumps.

As seen from Fig. 3, zeta potential values decreased as the pH of the medium increased. The negative charge density was higher for p(HEMA-APSA)−2 than for p(HEMA). The charge densities of p(HEMA) and p(HEMA-APSA)−2 hydrogels in the pH range of 2.0–11.0 ranged from 12.6 to −25.0 mV and 1.6 to −57.2 mV, respectively. The high negative charge densities of p(HEMA-APSA)−2 hydrogel compared to p(HEMA) were due to strong ion exchange sulfone groups of the APSA unit of the copolymer. The high negative zeta potential values of the copolymer at various pH could provide high adsorption performance for cationic CV and CR dyes compared to the homo-polymer.

The SEM micrographs provide evidence of the adsorbent's size, shape, and surface morphology. The surface morphologies of the p(HEMA) and p(HEMA-APSA)−2 hydrogels are presented in Fig. 4A and B. As observed in

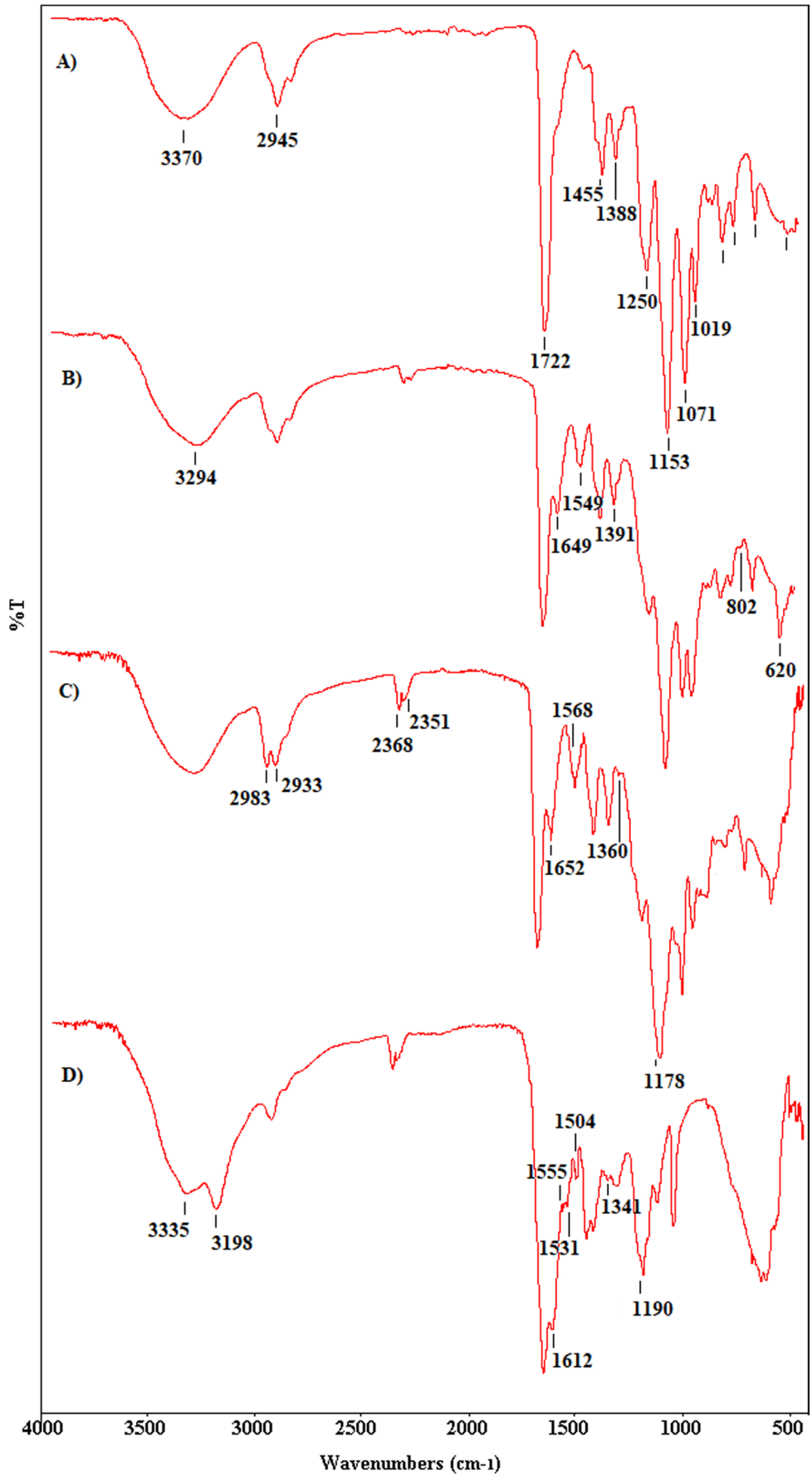

Fig. 2 FTIR spectra: (**A**) p(HEMA), (**B**) p(HEMA-APSA)−2, (**C**) p(HEMA-APSA)−2-CV, and (**D**) p(HEMA-APSA)−2-CR hydrogels

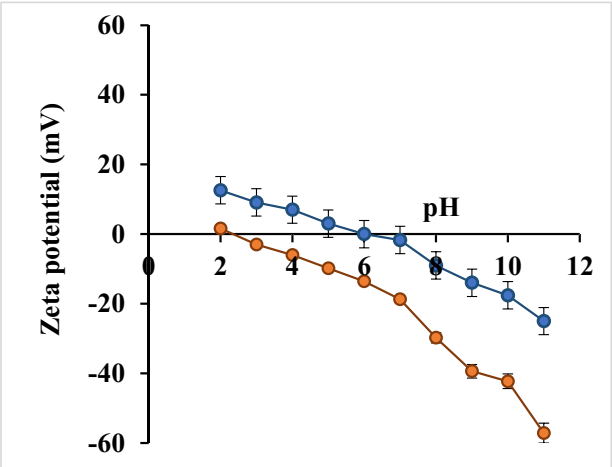

Fig. 3 The zeta potential values of p(HEMA) and p(HEMA-AMPSA)−2 hydrogels at different pH

Fig. 4A, a rough and highly irregular surface with some pores was obtained for p(HEMA) hydrogel. On the other hand, for the p(HEMA-APSA)−2 hydrogel, a structural change in the surface morphology was observed, suggesting that the incorporation of the APSA monomer was successfully achieved, and the surface of the p(HEMA-APSA)−2 was highly porous (Fig. 4B). This porous surface property provides a large surface area, so that the overall surface area can be significantly improved. Incorporating APSA monomer in the hydrogel structures can increase the contact surface area with the target molecules, and the adsorption capacity for the tested dyes increases. The particulate form of p(HEMA-APSA)−2 hydrogel is presented in Fig. 4C. The particles were in the adsorption studies.

Energy dispersive spectroscopy (EDS) studies of the p(HEMA-AMPSA)−2 were done to determine the change in the chemical composition of the adsorbent before and after adsorption of CR and CV dyes. Results of EDS analysis of the p(HEMA-AMPSA)−2, p(HEMA-AMPSA)−2-CR, and p(HEMA-AMPSA)−2-CV are presented in Fig. 5. As seen from Fig. 5, the atomic percentages of the p(HEMA-AMPSA)−2 hydrogel changed after adsorption of CR and CR dyes. As seen in Fig. 5, the atomic percentages of p(HEMA-AMPSA)−2 hydrogel changed after adsorption of CR and CR dyes. For p(HEMA-AMPSA)−2-CR, the percentages of nitrogen and sulfur were increased from 26.2 to 28.0% and from 0.1 to 1.3%, respectively, compared to pristine p(HEMA-AMPSA)−2 hydrogel. For p(HEMA-AMPSA)−2-CV, the percentage of nitrogen increased from 26.2 to 29.1% while the percentage of sulfur decreased from 0.2 to 0.1%. These results demonstrate that the elemental analysis obtained from EDS closely agrees with the interaction of CR and/or CV dyes with the p(HEMA-AMPSA)−2 starting composition used for synthesis. From the EDS analysis, no trace of any impurity was found in the tested samples, indicating the cleanness of the samples.

The p(HEMA) and p(HEMA-APSA)−1-3 hydrogels were ground using a mortar. 2.0 g of hydrogels were placed in the mortar and ground under wet conditions and dried in a vacuum oven. After drying, the grinding particles were sieved using a molecular sieve. The particles ≥ 75 µm were used in the adsorption tests. The surface areas of the p(HEMA) and p(HEMA-APSA)−2 hydrogels were obtained with nitrogen adsorption/desorption experiments. The surface area of the p(HEMA) particles was 2.45 g/m^2. Whereas the surface area of the p(HEMA-APSA)−2 particles was found to be 4.87 g/m^2, the copolymer's surface area was increased about two-fold compared to the homo-polymer.

Mechanical properties of the p(HEMA) and p(HEMA-APSA)−1-3 hydrogel formulations were studied within the equilibrium water content of each formulation. The tensile strength and percent break data of the hydrogel samples are presented in Table 2. These data showed that the mechanical properties of the p(HEMA) hydrogel sample were changed after incorporation of APSA in the hydrogel formulations.

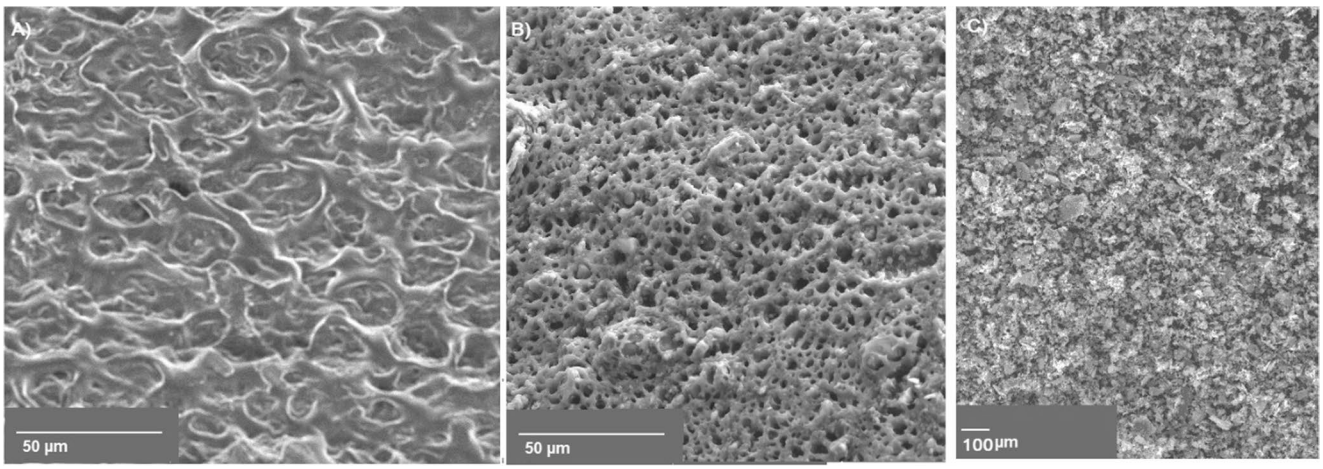

Fig. 4 SEM images: (**A**) p(HEMA), (**B**) p(HEMA-APSA)−2 and (**C**) particulates form p(HEMA-APSA)−2

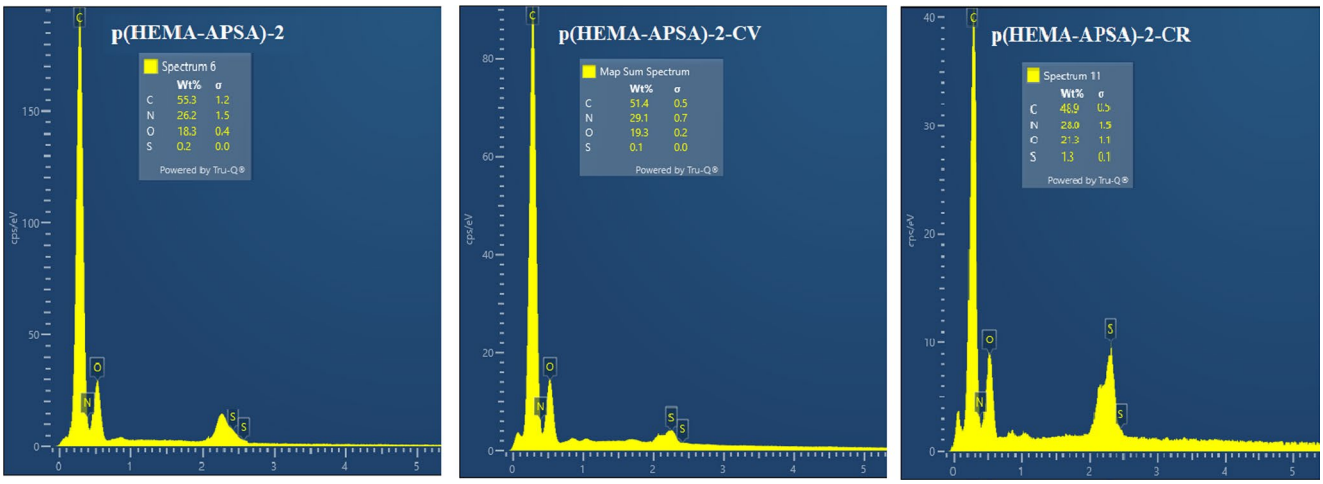

Fig. 5 Energy dispersive X-ray spectroscopy (EDS) analysis of the p(HEMA-AMPSA)−2 hydrogel sample before and after adsorption of CR and CV dyes

Table 2 Mechanical properties of p(HEMA) and p(HEMA-APSA)−1-3 hydrogel formulations

Formulation	Tensile strength (kPa)	Breaking strength (%)	Water Content (%)
p(HEMA)	207 ± 16	247 ± 10	136.3
p(HEMA-APSA)−1	198 ± 12	156 ± 13	382.4
p(HEMA-APSA)−2	172 ± 08	113 ± 10	751.9
p(HEMA-APSA)−3	98 ± 07	63 ± 05	1004.2

Table 3 APSA content, percent water content, and adsorption capacities to CR/CV dyes of the p(HEMA), and p(HEMA-APSA)−1, 2, and 3 hydrogels

Hydrogel formulation	APSA content (mmol/g)	Water content (%)	Adsorption capacity CV/CR (mg/g)
p(HEMA)	-	136.3	76.2/40.5
p(HEMA-APSA)−1	0.07	382.4	196.7/74.7
p(HEMA-APSA)−2	1.23	751.9	301.1/182.6
p(HEMA-APSA)−3	1.94	1004.2	367.4/204.8

As can be seen in Table 2, the tensile strength of p(HEMA-APSA)−1, p(HEMA-APSA)−2, and p(HEMA-APSA)−3 was decreased concerning their APSA content compared to the pure p(HEMA) hydrogel formulation, respectively. The reduction in the mechanical strength of the p(HEMA-APSA)−1, p(HEMA-APSA)−2, and p(HEMA-APSA)−3 could be due to the increasing water content of the hydrogel formulation, according to increased APSA compared to pure p(HEMA) hydrogel. As given in Table 2, as the APSA ratio was increased in the hydrogel formulations, a reduction in the elongation breaking percentage was observed for the tested hydrogel formulations. The p(HEMA-APSA)−2 formulation was used in the remaining studies because it has better operational mechanical properties and adsorption performance compared to p(HEMA-APSA)−3 and p(HEMA-APSA)−1, respectively, as given in Tables 2 and 3.

Effect of sulfone group density on adsorption performance

Removal of pollutants using adsorbents is based on the relationship of functional groups between target pollutants and the support surface. The amount of functional groups included on the adsorbent is a significant variable that can affect the adsorption efficacy of the target pollutant [42]. The influence of the amount of APSA monomer in the hydrogel formulations on the adsorption performance is shown in Table 3. An increase in the APSA monomer amounts from 0.068 to 1.94 led to a rise in the adsorption capacities of the hydrogel formulations for CV from 196.7 to 367.4 mg/g and CR from 74.7 to 204.8, respectively. The p(HEMA-APSA)−3 hydrogels have the maximum sulfone group density (containing 1.94 mmol/g) and resulted in higher CV and CR dyes adsorption capacity. Thus, when the sulfone groups' density increases, the available amount of functional groups that could interact with the tested dye molecules increases on the hydrogel's surface, leading to higher adsorption capacity. On the other hand, the p(HEMA-APSA)−3 had a high equilibrium water content of about 1004%, and due to its operational restriction, the p(HEMA-APSA)−2 hydrogel formulation with 750% equilibrium water content was used in the remaining adsorption studies.

Effect of adsorbent dosage

The amount of adsorbent in the adsorption medium has an important impact on the removal efficacy of the pollutant and plays an essential role in the cost assessment process. Therefore, determining adsorbent dosage could be a necessary parameter in adsorption studies as it could control the adsorption performance of an adsorbent for a known concentration

of pollutant [40, 43]. The adsorption of CV and CR dyes on the p(HEMA-APSA)−2 hydrogel was investigated by varying the adsorbent dosage to 50–500 mg/L while keeping the initial concentration of each dye at 50 mg/L. Figure 6 shows that the adsorption of CV and CR dyes increased rapidly with an increase in the amount of adsorbent and reached an equilibrium boundary after a limit. These could be explained by increasing the available adsorption sites in the medium as the adsorbent dosage increased. Whereas the adsorption capacity decreases with the increase in the adsorbent dosage. This tendency was seen for both CV and CR dyes. These may be related to the decrease in the amount of target contaminant adsorbed per gram of adsorbent with each successive increase in adsorbent dosage. It should be noted that the binding sites of the adsorbent could not be completely employed at a higher adsorbent dose in comparison to a lower adsorbent dose. The maximum removal was observed at a dosage of 250 mg/L for p(HEMA-APSA)−2 hydrogel to remove of 99.9% and 76.8% for CV and CR, respectively. Increasing the doses did not cause any change in the adsorption sites for CV dye, but a slight increase in the removal performance for CV up to 80.4% at 500 mg/L. Therefore, 250 mg/L of p(HEMA-APSA)−2 was used in the remaining experiments. Other researchers have reported similar results for dye removal by various adsorbents [43–45].

Effect of pH on adsorption of cationic dyes

The pH of the medium shows a significant role in the adsorption efficiency of the hydrogel adsorbent toward different dyes [34, 46–50]. The surface charges of the adsorbent are influenced by the initial pH of the adsorption medium, and the amount of dye ionization can also be altered. The removal performance of p(HEMA-APSA)−2 hydrogel to CV and CR was studied at different medium pH levels between 2.0 and 9.0. The results are presented in Fig. 7A. The dependency of CV and CR dye adsorption on pH is related to protonation/deprotonation of the functional groups of the surface of the hydrogels' adsorbent. At pH 2.0, the hydroxyl (–OH), carbonyl amide (–CONH), and sulfone ($–SO_3H$) functional groups in p(HEMA-APSA)−2 are protonated, where the dye binding sites compete with the hydrogen ions. On the other hand, at high pH values, hydroxyl, carbonyl amide, and sulfone functional groups are ionized; correspondingly, the adsorption of cationic dyes on the functional groups is more preferential. Thus, the tested cationic dyes adsorbed to the negatively charged surface sites of the hydrogel adsorbent. As seen in Fig. 7A, the maximum CV and CR dye removal was observed at pH 6.0 on the p(HEMA-APSA)−2 hydrogel, and the removal was reached 99.8% and 78.4%, respectively. As the control system p(HEMA) adsorbed 76.2 and 40.6% of CV and CR dyes, respectively. As observed from Fig. 7A, by decreasing or increasing the pH values below 6.0, the tendency to remove CV and CR dyes decreased. It should be remembered that the sulfone groups of the adsorbent dominated the electrostatic interactions with the positively charged surface of the dye molecules. These observations could be due to the protonation and deprotonation of functional groups on the adsorbent and the dye molecules. Furthermore, hydrogen bonds could be established between the dye molecules and the adsorbent as presented in Table 1. Thus, the adsorption of dyes on the adsorbent surface could be considered mainly through hydrogen bonding and electrostatic interactions.

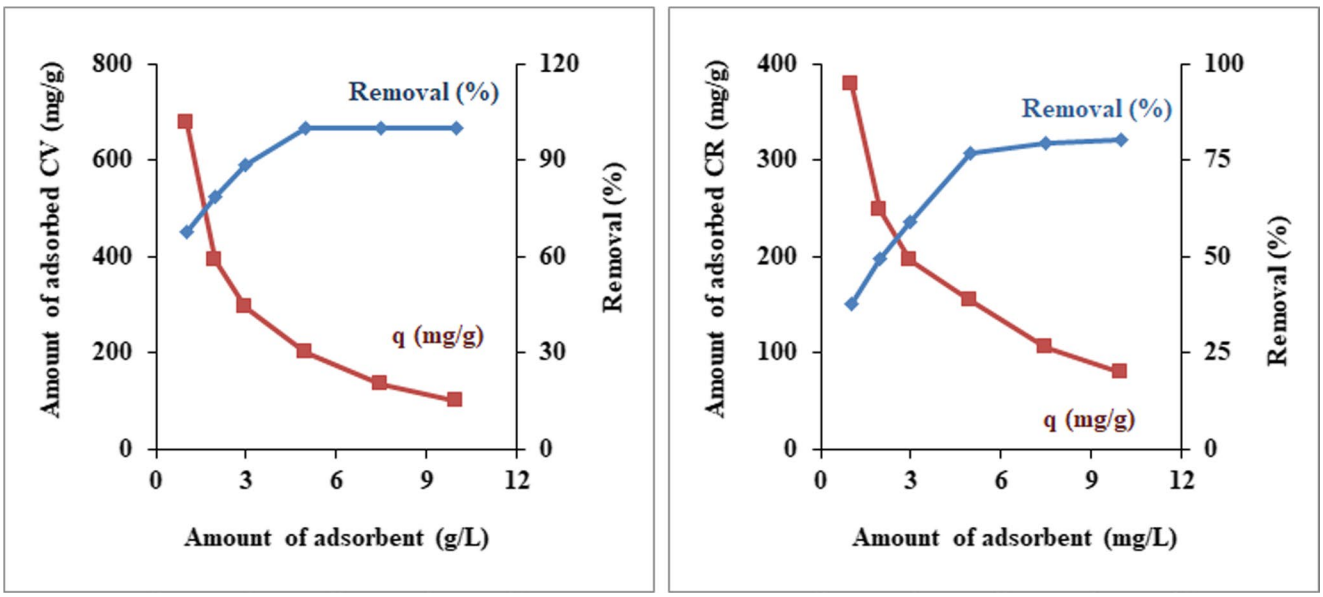

Fig. 6 The effect of the adsorbent dosage: CV and CR adsorption on p(HEMA-APSA)−2 hydrogel

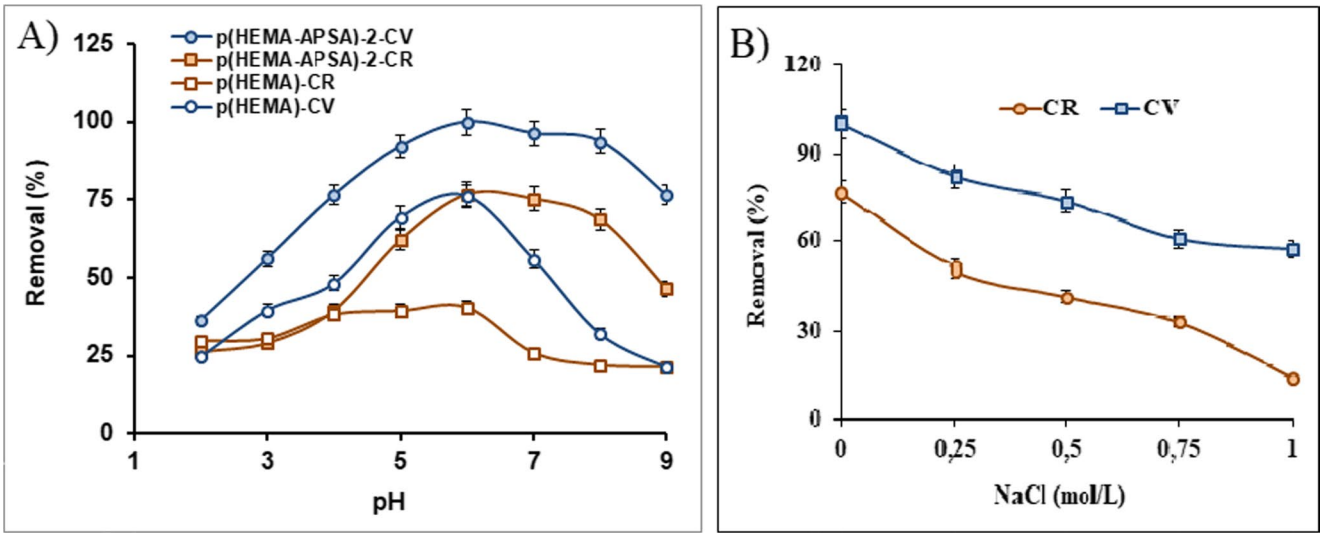

Fig. 7 Effect of pH on CV and CR adsorption p(HEMA-APSA)−2 (**A**); Effect of ionic strength on CV and CR removal process with p(HEMA-APSA)−2 hydrogel (**B**)

As given above, the surface charge variation under various pH values of p(HEMA) and p(HEMA-APSA)−2 was performed by studying zeta potential and pH_{ZPC} experiments (Fig. 3). The achieved zeta potential data and pH_{ZPC} studies for shown that the isoelectric points and zero point of charge of p(HEMA) and p(HEMA-APSA)−2 were approximately at pH 6.0 and 2.2, respectively. Therefore, p(HEMA-APSA)−2 displayed a neutral charge at pH 2.2 (pH_{ZPC}), and negative charges when greater than that of the pH_{ZPC} value. Accordingly, the negatively charged hydrogel adsorbent interacted with the tested cationic dye molecules, and showed about 99.8% and 78.4% removal efficacy for CV and CR dyes, respectively. Hereafter, based on the experimental outcomes for both dyes at varying pH media, pH 6.0 was designated as the optimal pH for further studies.

Effect of ionic strength

The effect of salt concentration on the removal efficiency of CV and CR dyes was examined by presenting increasing concentrations of NaCl (varying from 0.0 to 1.0 mol/L) under defined experimental conditions (pH: 6.0, initial concentration: 100 mg/L). Figure 7B shows the results achieved from these studies. As can be seen from this figure, the increasing of NaCl concentration from 0.0 to 1.0 mol/L, the percentage of removal of CV and CR dyes decreased from 99.8 to 56.7% and from 76.8 to 14.0%, respectively, which could be due to the competitive interactions between dye molecules and salt ions for binding sites during the adsorption process. The decrease of the adsorption capacity for CR was highly pronounced, about 82%, whereas this was 25% for CV dye. The increasing ionic strength (i.e., Na^+ and Cl^-) in the adsorption medium can shade the binding sites of the adsorbent, and the electric binary layers of the adsorbent surface are compressed, leading to a reduction in the electrostatic interactions [41, 42]. It should be noted that when the electrostatic forces between binding sites on the adsorbent and pollutant molecules are opposite, an increase in salt concentration can lead to a fast reduction in the adsorption performance of the adsorbent [40, 43]. It was worth mentioning that the removal performance of p(HEMA-APSA)−2 for CR was highly decreased at increasing salt concentration compared to CV dye, suggesting that the two primary amine groups of the CR dye could be highly shielded by salt molecules. These results showed that ion-exchange might be responsible for CR adsorption on the p(HEMA-APSA)−2 hydrogels.

Effect of coexisting cations on CV and CR adsorption

In the single system, the adsorption of CV and CR cationic dyes on p(HEMA-APSA)−2 hydrogels disclosed very good efficiencies. Therefore, the cationic metal ions such as Pb(II), Zn(II), Cu(II), Ni(II), and Ca(II) were selected to recognize the selectivity of the adsorbent. The selectivity of the adsorbent to CV and CR dyes was studied using a series of typical binary dye/metal ions systems. In the binary system, the tested metal ions and concentration of each dye were selected as 5.0 mol/L and 200 mg/L, respectively. The results of these experiments for CV and CR are presented in Fig. 8. The data elucidated that CV or CR dye was easily adsorbed by the p(HEMA-APSA)−2 adsorbent from binary medium even in the presence of competing metal ions. The adsorption efficacy of CV or CR dye in the different binary dye metal ions mixtures reached up to 76% and 63%, demonstrating that the p(HEMA-APSA)−2 adsorbent displayed

high selectivity to the tested dyes, respectively. It should be noted that the metal ion concentrations were approximately 17 and 10-fold higher than the CV and CR dye concentrations on a molar basis, respectively, in the binary mixture medium. These results delineated that the p(HEMA-APSA)−2 adsorbent has a strong affinity for the adsorption of the tested cationic dyes in the presence of various metal ions in each binary mixture. The order of metal ions and dye adsorption association was observed as Ca(II) > Pb(II) > Cu(II) > Ni(II) > Zn(II) and CV > CR, respectively. In the binary mixture, the p(HEMA-APSA)−2 adsorbent exhibited considerable adsorption capabilities for the CV and CR dyes, in the presence of various metal ions, at a 200 mg/L initial dye concentration. The p(HEMA-APSA)−2 adsorbent can be a favorable adsorbent for removing cationic dyes from wastewater. It was observed that the removal rate of CV and CR significantly reduced in the presence of Ca(II) and Pb(II) ions, which is attributed to the competitive adsorption for binding sites between dye molecules and coexisting ions [51, 52]. On the other hand, the removal efficiency of the dyes was slightly affected in the presence of Cu(II), Ni(II), and Zn(II) anions. These observations could result from different adsorption mechanisms for the dyes and the tested metal ions.

Effect of initial dye concentration

Studying the influence of initial dye concentration in solution is very important for discerning adsorption isotherms and kinetics and optimizing the performance of dye removal processes in different environmental applications. The effect of initial CV or CR dye concentration on the removal efficacy of the p(HEMA-APSA)−2 adsorbent was investigated in the 10–200 mg/L concentration range. Increasing the initial dye concentrations decreased CV and CR's removal efficiencies (Fig. 9A). There were sufficient available binding sites for CV or CR adsorption on the p(HEMA-APSA)−2 adsorbent at low starting dye concentrations. After 100 mg/L initial dye concentrations, the reduction of adsorption tendency of the tested dye could be due to the saturation of the adsorbent binding sites with dye molecules [43]. It should be noted that increasing the dye concentration in the medium enhances the driving force for mass transfer and overcomes the resistance of the surface separating the liquid from the solid. It was observed that this became significantly ineffective after the initial dye concentration of 150 mg/L, and there was no significant increase in the adsorbed amount of each of the tested dyes. In the process of removing CV and CR dyes from aqueous media with p(HEMA-APSA)−2 adsorbent, the maximum adsorption capacities at 25 °C were found to be 306.1 mg/g and 186.9 mg/g, respectively (Fig. 9).

Additionally, the experimental data were analyzed using two different isotherm models, namely Langmuir and the Freundlich isotherm models. The calculated isotherm constants from the fitted isotherm modeling are presented in Table 4.

The linearized Langmuir isotherm can be calculated by the following equation:

$$C_e/q_e = C_e/q_m + 1/bqm \quad (4)$$

where, q_e is the amount of adsorbed dye at equilibrium time (mg/g), C_e is the equilibrium concentration of dye in solution (mg/L), q_m represents the maximum adsorption capacity (mg/g), and b is the Langmuir constant related to the energy of adsorption (L/mg).

The essential properties of the Langmuir isotherm can be expressed by a dimensionless equilibrium parameter (R_L):

$$R_L = 1/(1 + bC_0) \quad (5)$$

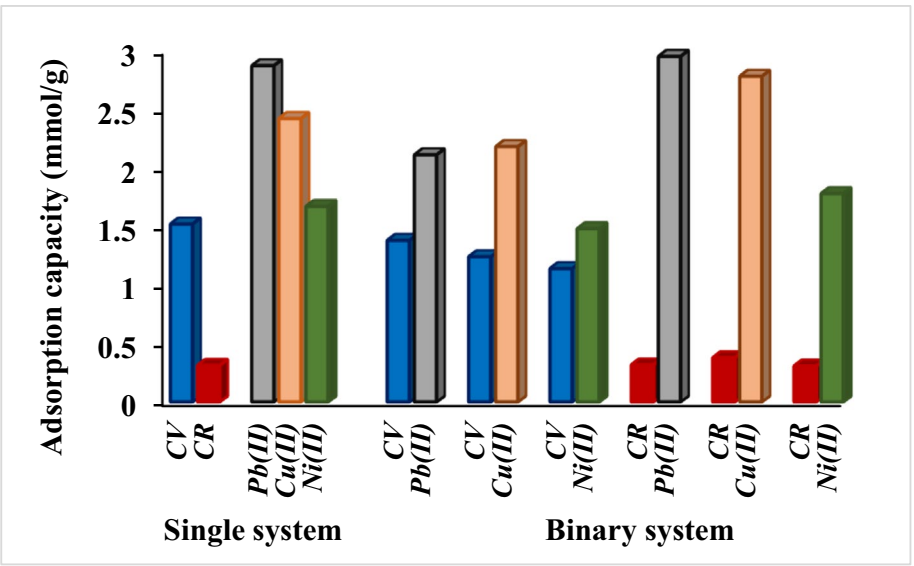

Fig. 8 Removal performance of p(HEMA-APSA)−2 hydrogel in single systems with for CV, CR, Pb(II), Cu(II) and Ni(II) and binary systems with CV/Pb(II), CR/Pb(II), CV/Cu(II), Cu(II)/CR, CV/Ni(II) and CR/Ni(II) dyes-metal ions

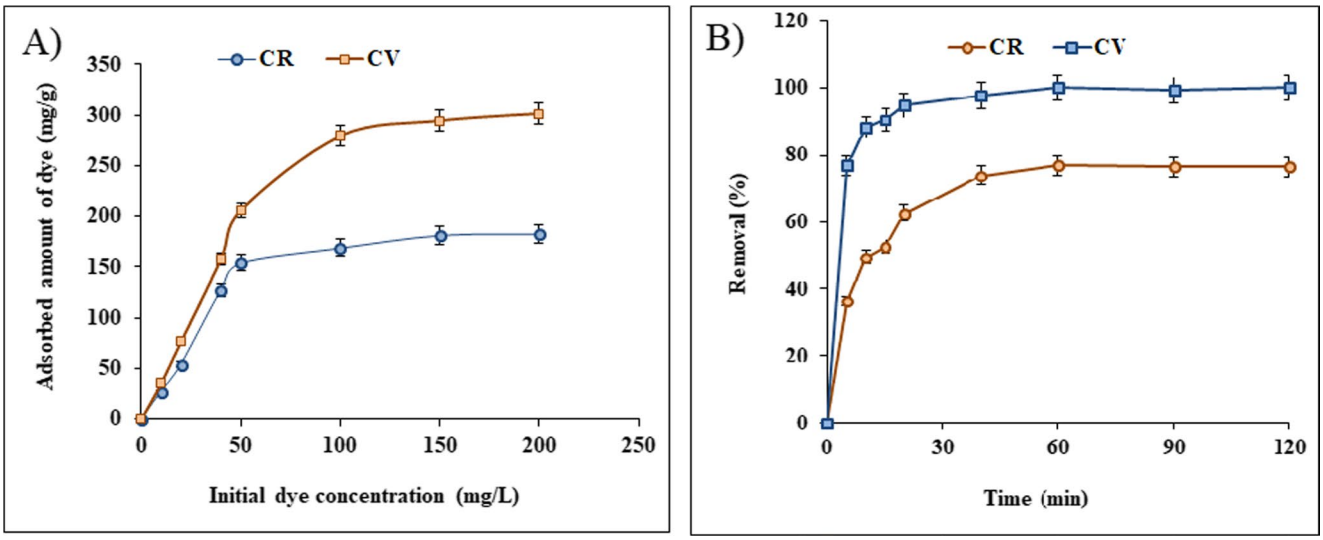

Fig. 9 Effect of initial dye concentration on CV and CR removal process with p(HEMA-APSA)−2 hydrogel (**A**): Effect of contact time on CV and CR adsorption on p(HEMA-APSA)−2 hydrogel (**B**)

Table 4 Langmuir and Freundlich isotherm model constants and correlation coefficients for the adsorption of CR and CV dyes on p(HEMA-APSA)−2 hydrogel

		Langmuir constants						Freundlich constants	
	T (K)	$q_{e,exp}$ (mg/g)	q_m (mg/g)	$bx10^{-5}$ (L/mol)	R^2	$^*R_L$	N	K_F	R^2
	288	141.6	161.7	0.338	0.989	0.094	2.06	15.59	0.858
	298	186.9	202.6	0.529	0.994	0.057	2.51	31.7	0.803
CR	308	242.8	250.5	1.360	0.999	0.025	3.10	60.5	0.827
	318	291.4	289.4	11.200	0.998	0.003	13.50	190.3	0.728
	288	198.7	235.4	0.171	0.992	0.107	1.83	17.2	0.914
CV	298	306.1	311.2	1.340	0.999	0.015	6.65	126.3	0.537
	308	384.2	387.3	2.090	0.998	0.009	8.29	175.6	0.609
	318	446.3	434.1	2.660	0.996	0.008	5.57	200.9	0.864

* C_0=200 mg/L

The linear form of the Freundlich adsorption isotherm can be expressed by the following equation:

$$\log\ q_e = \log\ K_F + 1/n\ \log\ C_e \quad (6)$$

where K_F and n are Freundlich constants.

It was observed that the experimental and q_m values of the p(HEMA-APSA)−2 adsorbent for CR and CV dyes were very close to each other at different temperatures. In addition, R^2 values were high for the Langmuir model in the range of 0.994–0.999 and 0.992–0.999 for the CR and CV dyes. These results show that the Langmuir isotherm model could well describe the adsorption of CR and CV dyes onto the p(HEMA-APSA)−2 adsorbent. The obtained q_m values from the Langmuir model equation suggested that p(HEMA-APSA)−2 adsorbent had remarkable maximum adsorption capacities of 202.6 and 311.2 mg/g for CR and CV dyes, respectively. These results propose that p(HEMA-APSA)−2 adsorbent could be highly effective for removing CV and CR dyes from solutions.

The Langmuir isotherm is also expressed in terms of the dimensionless separation factor R_L. The adsorption process is unfavorable when R_L is greater than 1, linear when R_L = 1, and irreversible when R_L is 0. For a proper adsorption process, the R_L value should be greater than 0 but less than 1. At 200 mg/L initial dye concentration, the R_L values were obtained in the range of 0.008–0.107 and 0.003–0.094 for CV and CR, respectively. These results show that the adsorption of CV and CR dyes onto the p(HEMA-APSA)−2 adsorbent is favorable and follows a monolayer adsorption process.

In the adsorption of CV and CR dyes onto the p(HEMA-APSA)−2 adsorbent, n values were found in the range of 1.83–8.29 for CV and 2.06–13.50 for CR. These results indicate a high adsorption tendency of dyes onto the adsorbent. The K_F values were between 15.6 and 190.3 for CR and 17.2 and 200.9 for CV with increasing temperature

from 288 to 318 K. The results indicate the facilitation of the adsorption process with increasing temperature and the high affinity of the adsorbent for both dyes.

Effect of contact time and adsorption kinetics of CV and CR dyes on adsorbent

Contact time is an important point for actual applications, as adsorption equilibrium time is an essential parameter to verify the appropriateness of the cost of the adsorbent for large-scale applications. Accordingly, the influence of contact time on the adsorption of CV and CR dyes on the p(HEMA-APSA)−2 hydrogel was studied, as the results are presented in Fig. 9B. The results showed that the p(HEMA-APSA)−2 hydrogel adsorbed CV and CR dyes in two separate phases. The early phase (0–20 min) was characterized by fast kinetics due to the considerable amount of dye in the medium and the many available binding sites on the surface of the p(HEMA-APSA)−2 hydrogel. The second phase, which lasted about 60 min, was slower due to the electrostatic repulsion caused by the adsorbed dye on the surface of the p(HEMA-APSA)−2 hydrogel and the dye molecules in the solution, and similarly, there was a significant decrease in the available binding sites on the adsorbent. The maximum adsorption amounts of CV and CR dyes were found to be 306.1 and 186.9 mg/g, respectively, and the equilibrium occurred after 60 min. The order of the adsorption capacities of the dyes was CV > CR, and the maximum adsorption was obtained with a contact time of 120 min, indicating that the p(HEMA-APSA)−2 hydrogel could be a favorable adsorbent to remove cationic dyes from aqueous solution.

The kinetics of CV and CR dye adsorption on p(HEMA-APSA)−2 were investigated using pseudo-first and pseudo-second-order models, and the kinetic parameters are given in Table 5.

The linearized form of the pseudo-first-order model can be expressed as follows:

$$\log\left(q_e - q_t\right) = \log\ q_e - k_1/2.303 \tag{7}$$

where q_t is the amount of adsorbate adsorbed per unit mass of adsorbent at time t (mg/g), k_1 is the pseudo-first-order rate constant (per min), and t is the contact time (min).

The pseudo-second-order equation is expressed as:

$$t/q_t = 1/k_2 q_e{}^2 + t/q_e \tag{8}$$

where k_2 and q_e are the pseudo-second order rate constant (g/mg/min) and equilibrium adsorption capacity, respectively.

The adsorption initial rate constant is denoted by h and is defined by $h = k_2 q_e{}^2$ [53–56]. As can be seen from Table 5, the pseudo-second-order kinetic model shows higher R^2 values than the first-order model. In addition, while the q_e values obtained for the pseudo-first-order kinetic model do not match the experimental q_e values, the q_e values obtained for the pseudo-second-order model match better with the experimental values. This shows that the pseudo-second-order kinetic model could explain the adsorption of both dyes to the p(HEMA-APSA)−2 hydrogel.

Thermodynamics parameters

The influence of temperature on the adsorption of CV and CR dyes from the aqueous medium on p(HEMA-APSA)−2 hydrogel is a critical factor for evaluating temperature-dependent dye adsorption mechanisms. The effect of temperature on the adsorption process of CV and CR dyes from aqueous medium by the p(HEMA-APSA)−2 hydrogel was investigated in the 288–318 K range. The adsorption capacity of the p(HEMA-APSA)−2 hydrogel increased with increasing temperature from 288 to 318 K, and the amount of adsorbed CV and CR dyes increased from 198.7 to 446.3 and from 141.6 to 291.4 mg/g, respectively (Table 6). This could be due to the increase in the number of available binding sites on the p(HEMA-AMPSA)−2 hydrogel surface by expanding the polymeric network with the increase in temperature.

Thermodynamic parameters such as standard free energy change (ΔG^o), standard enthalpy change (ΔH^o), and standard entropy change (ΔS^o) were determined and calculated using the following equations to evaluate the feasibility, direction, and nature of the adsorption process of dyes onto the adsorbent.

$$\triangle G^\circ = -RT\ln K_a \tag{9}$$

$$\ln K_a \triangle S^\circ/R - \triangle H^\circ/RT \tag{10}$$

The equilibrium constants b (K_a) for the adsorption of CV and CR dyes onto the adsorbent were determined from the

Table 5 First and second order kinetic model constants and correlation coefficients for adsorption of CV and CR dyes on p(HEMA-APSA)−2 hydrogel

		First order			Second order			
	q_{exp} (mg/g)	q_{eq} (mg/g)	$k_1 \times 10^2$ (min^{-1})	R^2	q_{eq} (mg/g)	$k_2 \times 10^3$ (g/mg min)	R^2	h (mg/g min)
CR	186.9	394.5	13.0	0.978	198.8	0.08	0.999	33.0
CV	306.1	126.3	7.76	0.981	313.9	1.29	0.998	127.4

Table 6 Thermodynamic parameters calculated for the adsorption process of model CR and CV dyes with p(HEMA-APSA)−2 hydrogel

	T (K)	ΔG° (kJ/mol)	ΔS° (kJ/mol K)	ΔH° (kJ/mol)
CR	288	−25.0	0.37	85.7
	298	−27.1		
	308	−30.3		
	318	−36.8		
CV	288	−23.3	0.31	66.9
	298	−29.3		
	308	−31.4		
	318	−33.0		

Langmuir equation at four different temperatures (Table 4). Thermodynamic parameters ΔH° and ΔS° were determined from the slope and cut-off point of the 1/T − 1/T-lnK_a graph according to the van't Hoff equation, respectively. As can be seen from Table 6, ΔG° values decrease from − 23.3 to −38.0 and from − 25.0 to −36.8 for CV and CR dye, respectively, as the temperature increases from 288 K to 318 K. The negative ΔG° values show that the adsorption process of CV and CR dyes on the adsorbent occurred spontaneously. In addition, the decreasing ΔG° values with increasing temperature show that temperature increases the absorption driving force, and high temperature is suitable for adsorption. The ΔH° values for the adsorption of CV and CR dyes on the adsorbent were found to be 85.7 and 66.9 kJ/mol, respectively (Table 6). Positive ΔH° values indicate that the adsorption process is endothermic. Therefore, an increase in temperature leads to a higher dye adsorption at equilibrium. The ΔS° values for the adsorption of CV and CR dyes on the adsorbent were determined as 0.373 and 0.311 kJ/mol K, respectively. The positive values of ΔS° indicated that the adsorption of dyes on the adsorbent was spontaneous, and the randomness increased during the adsorption process [56–58].

Desorption and reusability studies

Reusability is one of the important parameters of adsorbent performance and is related to desorption/regeneration cycles. An adsorbent's physical and chemical structure is expected to stay intact throughout the adsorption-desorption process. Therefore, selecting the adsorbent is crucial in this respect [59, 60]. The desorption efficiencies of the CV or CR loaded adsorbent were studied using 0.1 mol/L NaOH as desorbing agents. The adsorption-desorption cycle was repeated five times with the same adsorbent sample to demonstrate reusability. It was found that the adsorption capacity of the p(HEMA-AMPSA)−2 hydrogel decreased by 5.6% and 13.8% for the CV and CR dyes after five repeated adsorption-desorption cycles, respectively. The adsorbent indicated good regeneration efficiency, and a minor decrease in adsorption capacity was found during the five adsorption-desorption cycles. The results show that the reusability of the adsorbent was promising in terms of both applicability and economic point of view.

Comparison of the adsorption capacity of the p(HEMA-APSA)−2 for CV and CR with previously reported work

It is critical to compare the adsorption capacity of the prepared adsorbent to that of the reported adsorbents for their environmental applications. The adsorption capacities of the earlier reported adsorbents are compared to the hydrogel adsorbent presented in this work, and given in Table 7. As seen in the table, it was observed that the adsorption capacity of p(HEMA-APSA)−2 hydrogel adsorbent for Crystal Violet (306.1 mg/g) and Congo Red (189.6. mg/g) dyes was higher compared to the adsorption capacities of most of the available adsorbents available in the literature [19, 58] [61–74]. These observations could be attributed to the sufficiency of the interactions between the tested cationic dye molecules and sulfate groups of the p(HEMA-APSA)−2 hydrogel adsorbent. The strong cationic p(HEMA-APSA)−2 adsorbent could be considered favorable for removing CV and CR dyes from aqueous solutions. The high adsorption capacity of p(HEMA-APSA)−2 hydrogel for CV dye relative to CR dye can be attributed to the three tertiary amine groups of CV and the sulfone groups on the copolymer chains.

Conclusions

Due to their harmful properties, the removal of various inorganic and organic pollutants from the environment and wastewaters has been a topic of remarkable interest in recent years. Sulfone groups containing anionic hydrogel adsorbent were produced using APSA and HEMA monomers via redox polymerization to achieve this goal. The p(HEMA-APSA)−2 hydrogel revealed good performance in adsorbing CV and CR dyes from aqueous solutions, attaining maximum adsorption capacities under defined adsorption conditions. At a pH of 6.0, a contact time of 120 min, and initial concentrations of 200 mg/L for CV and CR, the maximum adsorption capacities reached 306.6 mg/g and 186.9 mg/g, respectively. Moreover, remarkable results were obtained for CV and CR removal with various amounts of functional -SO_3H groups. A rapid adsorption occurred within 20 min for both CV and CR dyes. The p(HEMA-APSA)−2 hydrogel adsorption processes for the CV and CR dyes were described by pseudo-second-order kinetics. The adsorption of CV and CR dyes was associated with different interaction

Table 7 Comparison of the adsorption capacities of various adsorbents to CV and CR dyes with the presented investigation

Adsorbent	Dye/Adsorption capacity (mg/g)	pH	References
GO-carboxymethyl tamarind	CV/111	7.0	[58]
Sulfonated guar gum-hydrogels	CV/45.6	6.0	[61]
Nanocellulose-polyurethane	CV/41.6	10	[63]
Eggshell/hydroxyapatite/chitosan	CV/93.1	8.0	[64]
Poly(MAA-ko-AAm))/bentonite	CV/149.3	7.0	[65]
TiO_2-inulin-Fe_3O_4	CV/89.2	6.0	[66]
Cell-g-AASO_3H-co-AN	CV/44.1	7.0	[67]
Hydrogel nanocomposite	CV/155.0	7.0	[68]
Cyclodextrin- thiacalix [4]arene	CV/6.8	6.0	[69]
p(HEMA-APSA)−2 hydrogel	CV/306.1	6.0	In this work
Nylon fiber waste	CR/188.0	6.0	[19]
Fe_3O_4@SiO_2/PEI	CR/134.6	6.0	[62]
Eggshell/hydroxyapatite/chitosan	CR/98.4	6.0	[64]
Fe_3O_4@St-AcANCH	CR/72.8	5.0	[70]
Magnetic chitosan microsphere	CR/30.0	7.0	[71]
Magnetic chitosan	CR/192.9	4.0	[72]
S. latifolium biorefinery waste	CR/21.0	5.0	[73]
Triazine-based porous polymer	CR/103.0	6.0	[74]
p(HEMA-APSA)−2 hydrogel	CR/189.6	6.0	In this work

mechanisms, including hydrogen bonding, ion-exchange, and electrostatic interaction, which fitted the Langmuir model. An endothermic and feasible adsorption process was established by employing thermodynamic properties. In the metals and dyes systems, competition between metal ions and cationic dyes for adsorption sites on the adsorbent was very effective, and the adsorption performance of the adsorbent was decreased for the tested dyes. Furthermore, the adsorption performance of the p(HEMA-APSA)−2 hydrogel was maintained at about 87% and 79% for CV and CR dyes after five consecutive adsorption-desorption cycles. Finally, p(HEMA-APSA)−2 hydrogel was effectively applied to remove two cationic dyes in aqueous solution.

Acknowledgements The authors are very grateful to the Biochemical Processing and Biomaterial Research Laboratory, Gazi University, TURKEY, for providing basic instrumental and research facilities for this research.

Author contributions "G.B. Conceptualization, validation, investigation, wrote the main manuscript text, writing– review & editing; M.K. Investigation and prepared all figures and tables. I.A.-E. Investigation, validation; O.H. Investigation, M.Y.A. Conceptualization, Writing - review & editing. All authors reviewed the manuscript."

Funding Not applicable.

Data availability No datasets were generated or analyzed during the current study.

Declarations

Consent for publication All authors have given consent for publication.

Competing interests The authors declare that they have no known competing financial interests or personal relationships that could have appeared to influence the work reported in this paper.

References

1. Li S, Liang Y, Li Q, He Y (2024) Easily recyclable magnetic polyacrylamide/sodium alginate/fe. J Polym Res 31:359. https://doi.org/10.1007/s10965-024-04195-x
2. Tirkey N, Mishra S (2025) Evaluation of Neem gum-poly(acrylic acid) based adsorbent for cationic dye removal using adsorption isotherm, kinetics and thermodynamics: linear regression models. Int J Biol Macromol 307:142059. https://doi.org/10.1016/j.ijbiomac.2025.142059
3. Arica TA, Ayas E, Arica MY (2017) Magnetic MCM-41 silica particles grafted with poly(glycidylmethacrylate) brush: modification and application for removal of direct dyes. Micropor Mesopor Mater 243:164–175. https://doi.org/10.1016/j.micromeso.2017.02.011
4. Al-Niaeem HS, Abdulwahid AA, Hanoosh WS (2021) Removal of carcinogenic dyes congo red (cr) and Bismarck brown y (bby) by adsorption onto reusable hydrogels derived from acrylamide. J Phys: Conf Ser 2063:012011. https://doi.org/10.1088/1742-6596/2063/1/012011
5. Arica TA, Balci FM, Balci S, Arica MY (2022) Highly porous poly(*o*-phenylenediamine) loaded magnetic carboxymethyl cellulose hybrid beads for removal of two model textile dyes. Fibers Polym 23:2838–2854. https://doi.org/10.1007/s12221-022-0221-4
6. Liu P, Bi Y, Mao J, Zhang J, Gu Y, Yunxue L (2024) High-performance calcium alginate hydrogel composite nanofiltration membrane for dyeing wastewater separation. J Polym Res 31:377. https://doi.org/10.1007/s10965-024-04229-4
7. Akköz Y, Coşkun R (2023) Cellulose-supported bioadsorbent from natural hemp fiber for removal of anionic dyes from aqueous solution. Int J Biol Macromol 252:126447. https://doi.org/10.1016/j.ijbiomac.2023.126447
8. Haleem A, Pan JM, Shah A, Hussain H, He WD (2023) A systematic review on new advancement and assessment of emerging

polymeric cryogels for environmental sustainability and energy production. Sep Pur Technol 316:123678. https://doi.org/10.1016/j.seppur.2023.123678
9. Naga N, Kusakabe M, Nakano T (2025) Synthesis and morphology control of a tetra-functional epoxy/polyethylenepolyamine monolithic porous polymers aspiring to selective molecular adsorption. J Polym Res 32:29. https://doi.org/10.1007/s10965-025-04254-x
10. Zhu L, Guan C, Zhou B, Zhang Z, Yang R, Tang Y, Yang J (2017) Adsorption of dyes onto sodium alginate graft poly(acrylic acid-*co*-2-acrylamide-2-methyl Popane sulfonic acid)/ Kaolin hydrogel composite. Polym Polym Compos 25:627–634. https://doi.org/10.1177/096739111702500808
11. Dastyar F, Dinari M (2024) Preparation of pyridine based porous organic polymers as new adsorbents to remove congo red dye from aqueous media. J Polym Res 31:315. https://doi.org/10.1007/s10965-024-04166-2
12. Arica TA, Kuman M, Gercel O, Ayas E (2019) Poly(dopamine) grafted bio-silica composite with tetraethylenepentamine ligands for enhanced adsorption of pollutants. Cheml Eng Res Des 141:317–327. https://doi.org/10.1016/j.cherd.2018.11.003
13. Bo C, Tang X, Jia Z, Li Y, Gong B, Ma X, Dai X (2024) Preparation of copolymer brush-type restricted access microspheres with adjustable adsorption selectivity to variety of dyes. J Appl Polym Sci 141:e54884. https://doi.org/10.1002/app.54884
14. Brandão WQ, Maciel BG, de Araújo Lima EM, Mojica-Sánchez LC, da Silva RJ, de Melo CP (2023) Carboxymethyl cellulose magnetic composite for adsorptive removal of cationic toluidine blue dye. Mater Chem Phys 303:127782. https://doi.org/10.1016/j.matchemphys.2023.127782
15. Khan ZA, Elwakeel KZ, Mashabi RA, Elgarahy AM (2023) Adsorption of anionic dyes onto 1,5-Diphenylcarbazide functionalized magnetic hybrid polymer: impact of water salinity and surfactants on adsorption isotherms. J Ind Eng Chem 131:569–584. https://doi.org/10.1016/j.jiec.2023.10.061
16. Bayramoglu G, Salih B, Akbulut A, Arica MY (2019) Biodegradation of cibacron blue 3GA by insolubilized laccase and identification of enzymatic byproduct using MALDI-ToF-MS: toxicity assessment studies by Daphnia magna and Chlorella vulgaris. Ecotox Environ Safe 170:453–460. https://doi.org/10.1016/j.ecoenv.2018.12.014
17. Bayramoglu G, Angi SB, Acikgoz-Erkaya I, Arica MY (2022) Preparation of effective green sorbents using *O. Princeps* Alga biomass with different composition of amine groups: comparison to adsorption performances for removal of a model acid dye. J Mol Liq 347:118375. https://doi.org/10.1016/j.molliq.2021.118375
18. Figueiredo VV, Vianna ELF, Lima BS, Jesus TCL, García-Vill´en F, Bertolino LC, Spinelli LS, Viseras C (2023) Brazilian Palygorskite as an alternative to commercial adsorbents for methylene blue: A discussion about composition, morphology and pore profile. Micropor Mesopor Mater 366:112957. https://doi.org/10.1016/j.micromeso.2023.112957
19. Hamad KH, Yasser AM, Nabil R, Tarek R, Hesham E, El-Telbany A, Saeed A, Selim SE, Abdelhamid AE, Abdelhamid AE (2024) Nylon fiber waste as a prominent adsorbent for congo red dye removal. Sci Rep 14:1088. https://doi.org/10.1038/s41598-023-51105-0
20. Arica MY, Salih B, Celikbicak O, Bayramoglu G (2017) Immobilization of laccase on the fibrous polymer-grafted film and study of textile dye degradation by MALDI–ToF-MS. Chem Eng Res Des 128:107–119. https://doi.org/10.1016/j.cherd.2017.09.023
21. Kumawat YK, Nair A, Choudhary S, Sharma JNK, Rasool T, Yogendra VS, Mishra K, Kumar V (2024) Novel hydrogel based on natural hybrid backbones: optimized synthesis and effective adsorbent for the removal of malachite green dye from an aqueous solution. J Polym Res 31:128. https://doi.org/10.1007/s10965-024-03973-x
22. Mello BL, Thue PS, da Silva PV, Machado FM, Naushad M, Sellaoui L, Badawi M, dos Reis GS, Dotto GL, Lima EC (2024) Grafting 3-trimethoxysilylpropyl)diethylenetriamine on microcrystalline cellulose for the adsorption of dyes: experimental and modeling studies. React Funct Polym 196:105836. https://doi.org/10.1016/j.reactfunctpolym.2024.105836
23. Phonlakan K, Meetam P, Chonlaphak R, Kongseng P, Chantarak S, Budsombat S (2023) Poly(acrylic acid-*co*-2-acrylamido-2-methyl-1- propanesulfonic acid)-grafted Chitosan hydrogels for effective adsorption and photocatalytic degradation of dyes. RSC Adv 13:31002–31016. https://doi.org/10.1039/D3RA05596E
24. Kapase SA, Patil PH, Jadhav SA (2025) Recent advancements in polyethyleneimine (PEI)-grafted materials and composites as versatile adsorbents for water detoxification. Macromol Res 33:249–270. https://doi.org/10.1007/s13233-024-00356-5
25. Qin X, Meng W, Cheng S, Xing B, Shi C, Nie Y, Wang Q, Xia H (2023) Efficient removal of heavy metal and antibiotics from wastewater by phosphate-modified hydrochar. Chemosphere 345:140484. https://doi.org/10.1016/j.chemosphere.2023.140484
26. Ristić M, Samaržija-Jovanović S, Jovanović T, Jovanović V, Kostić M, Marković G, Marinović-Cincović M (2023) Organically modified montmorillonite as an environmental adsorbent of pollutants: formaldehyde from urea-formaldehyde resin and acid red 183 dye from the aqueous solution. J Environ Chem Eng 12:111828. https://doi.org/10.1016/j.jece.2023.111828
27. Bora A, Karak N (2023) Biobased hydrogel reinforced with wastepaper-derived modified cellulose nanofiber as an efficient dye remover from wastewater. J Polym Res 30:452. https://doi.org/10.1007/s10965-023-03828-x
28. Cai Y, Qiu C, Yang K, Tian B, Bi Y (2024) Adsorption–degradation of methylene blue by natural manganese ore: kinetics, characterization, and mechanism. Int J Environ Sci Technol 21:1817–1830. https://doi.org/10.1007/s13762-023-05024-2
29. Chopra L, Sharma A, Chohan JS, Upadhyay VV, Singh R, Sharma S, Dwivedi SP, Kumar A, Tag-Eldin EM (2023) Synthesis and characterizations of super adsorbent hydrogel based on biopolymer, Guar Gum-grafted-Poly (hydroxyethyl methacrylate) (Gg-g-poly(HEMA)) for the removal of Bismarck brown Y dye from aqueous solution. Int J Biol Macromol 256:128518. https://doi.org/10.1016/j.ijbiomac.2023.128518
30. Anush SM, Kaliprasad CS, Gowda GPH, Gayathri BH, Girish YR, Prashantha K, Ramasundaram S, Altaf M, Oh TH, Durai M (2024) Pyrazine substituted chitosan: an adsorbent material for the efficient removal of anionic dyes from aqueous solutions. J Polym Res 31:320. https://doi.org/10.1007/s10965-024-04173-3
31. Wu L, Mingyang S, Ronghui G, Dong W (2022) Development of a novel pullulan/polydopamine composite hydrogel adsorbent for dye removal. Colloid Surf A: Physicochem Eng Aspect 652:129632. https://doi.org/10.1016/j.colsurfa.2022.129632
32. Radia ND, Aljeboree AM, Mhammed AAA (2024) Enhanced removal of crystal Violet from aqueous solution using Carrageenan hydrogel nanocomposite/mwcnts. Inorg Chem Commun 167:112803. https://doi.org/10.1016/j.inoche.2024.112803
33. Kumari B, Chauhan S, Kumar K, Singh S, Chauhan GS (2025) Simultaneous removal of cationic and anionic dyes from a complex mixture using a novel composite hydrogel based on pine needles, chitosan, and gelatin. Int J Biol Macromol. https://doi.org/10.1016/j.ijbiomac.2025.141447
34. Li Y, Qu G, Zhang H, Xie L, Zhang Y-F (2024) pH-Responsive removal of dyes from wastewater using MXene composited L-Cysteine-grafted HEMA hydrogel: dynamics, selectivity, regeneration and mechanism. Chem Eng Sci 300:120648. https://doi.org/10.1016/j.ces.2024.120648

35. Atay NO, Akgol S (2024) Fabricating polymeric hydrogel membranes embedded with amine and copper– modified nanostructures for RG 19 removal. Colloid Polym Sci 302:303–315. https://doi.org/10.1007/s00396-023-05195-x
36. Njuguna D, Schonherr H (2024) Tunable Gellan gum hydrogels as high capacity adsorbents for rapid dye removal. ACS Appl Polym Mater 6:1528–1539. https://doi.org/10.1021/acsapm.3c02761
37. Wang Y, Zhao L, Peng H, Wu J, Liu Z, Guo X (2016) Removal of anionic dyes from aqueous solutions by cellulose-based adsorbents: equilibrium, kinetics, and thermodynamics. J Chem Eng Data 61:3266–3276. https://doi.org/10.1021/acs.jced.6b00340
38. Guo J, Zhou S, Ma X, He S, Chen D, Xie F, Wang C, Yang H, Li W (2023) Regenerated cellulose/polyethyleneimine composite aerogel for efficient and selective adsorption of anionic dyes. Sep Purif Technol 330:125480. https://doi.org/10.1016/j.seppur.2023.125480
39. Pervez MN, Hassan MM, Naddeo V (2023) Separation of cationic methylene blue dye from its aqueous solution by S-sulfonated wool keratin-based sustainable electrospun nanofibrous membrane biosorbent. Sep Purif Technol 333:125903. https://doi.org/10.1016/j.seppur.2023.125903
40. Bayramoglu G, Arica MY (2021) Grafting of regenerated cellulose films with fibrous polymer and modified into phosphate and sulfate groups: application for removal of a model azo-dye. Colloid Surf A: Physicochem Eng Aspect 614:26173. https://doi.org/10.1016/j.colsurfa.2021.126173
41. Bayramoglu G, Kilic M, Arica MY (2023) *Tramates trogii* biomass in carboxymethylcellulose-lignin composite beads for adsorption and biodegradation of bisphenol A. Biodegradation 34:263–281. https://doi.org/10.1007/s10532-023-10024-7
42. Bayramoglu G, Denizli A, Arica MY (2002) Membrane with incorporated hydrophobic ligand for hydrophobic interaction with proteins: application to lipase adsorption. Polym Int 51:966–972. https://doi.org/10.1002/pi.899
43. Bayramoglu G, Tilki S, Arica MY (2024) Preparation of amine or carboxyl groups modifed cellulose beads for removal of uranium (VI) ions from aqueous solutions. Cellulose 31:5133–5149. https://doi.org/10.1007/s10570-024-05909-6
44. Roa K, Oyarce E, Boulett A, Samman ALM, Oyarzún D, Pizarro GDC, Sánchez J (2021) Lignocellulose-based materials and their application in the removal of dyes from water: A review. Sustain Mater Technol 29:e00320. https://doi.org/10.1016/j.susmat.2021.e00320
45. Vijayasree VP, Manan NSA (2023) Magnetite carboxymethylcellulose as biological macromolecule-based absorbent for cationic dyes removal from environmental samples. Int J Biol Macromol 242:124723. https://doi.org/10.1016/j.ijbiomac.2023.124723
46. Jain SN, Bhandari PS, Bodkhe M, Chavan G, Korade O, Parmar M, Daware GB, Gautam NB (2024) Adsorptive separation of Acid Red 33 by groundnut shell–based activated carbon. Biomass Conv Bioref. https://doi.org/10.1007/s13399-024-06424-1
47. Liu Y, Qiu G, Liu Y, Niu Y, Qu R, Ji C, Whang Y, Zhang Y, Sun C (2022) Fabrication of CoFe-MOF materials by different methods and adsorption properties for congo red. J Mol Liq 360:119405. https://doi.org/10.1016/j.molliq.2022.119405
48. Muhammadi H, Ghorbanloo M, Masami M, Yahiro H (2022) Adsorption of cationic dye from aqueous solutions by green ph responsive hydrogels based on poly(2-acrylamido-2-methyl-1-propanesulfonic acid). Nanochem Res 7:107–121. https://doi.org/10.22036/ncr.2022.02.006
49. Njuguna D, Schönherr H (2024) Tunable Gellan gum hydrogels as high capacity adsorbents for rapid dye removal. ACS Appl Polym Mater 6:1528–1539. https://doi.org/10.1021/acsapm.3c02761
50. Wang B, Luan L, Li Z, Wang J, Liu Y, Niu Y, Chen H (2024) Synthesis of heterostructured microspheres for efficient removal of malachite green and basic Fuchsine. Chem Eng Sci 303:120956. https://doi.org/10.1016/j.ces.2024.120956
51. Usman M, Ahmed A, Yu B, Wang S, Shen Y, Cong H (2021) Simultaneous adsorption of heavy metals and organic dyes by β-Cyclodextrin-Chitosan based cross-linked adsorbent. Carbohydr Polym 255:117486. https://doi.org/10.1016/j.carbpol.2020.117486
52. Waqeel J, Khan ST (2025) Empirical modelling based optimization of azo-dye adsorption by polyurethane sponge containing sodium alginate-TiO_2-NPs for small scale industry. Water Air Soil Pollut 236:175. https://doi.org/10.1007/s11270-025-07813-6
53. Sarvalkar PD, Vadanagekar AS, Karvekar OS, Kumbhar PD, Terdale SS, Thounaojam AS, Kolekar SS, Vhatkar RS, Patil PS, Sharma KKK (2023) Thermodynamics of Azo dye adsorption on a newly synthesized titania-doped silica aerogel by cogelation: a comparative ınvestigation with silica aerogels and activated charcoal. ACS Omega 8:13285–13299. https://doi.org/10.1021/acsomega.3c00552
54. Yang H, Wu K, Zhu J, Lin Y, Ma X, Cao Z, Ma W, Gong F, Liu C, Pan J (2024) Highly efficient and selective removal of anionic dyes from aqueous solutions using polyacrylamide/peach gum polysaccharide/attapulgite composite hydrogels with positively charged hybrid network. Int J Biol Macromol 266:131213. https://doi.org/10.1016/j.ijbiomac.2024.131213
55. Kapase SA, Patil PH, Jadhav SA (2025) Recent advancements in polyethyleneimine (PEI)-grafted materials and composites as versatile adsorbents for water detoxification. Macromol Res. https://doi.org/10.1007/s13233-024-00356-5
56. Wang J, Che K, Yang P, Cui T, Wan Y, Yang Z, Zhang Q (2024) A simple method to synthesize threedimensional network adsorbent of nanocellulose dispersed $Fe(OH)_3$ for enhanced adsorption of congo red. Fibers Polym 25:4575–4586. https://doi.org/10.1007/s12221-024-00762-7
57. Yamada K, Terada S, Yamamoto R, Anh DC, Naitou T, Yamamoto S (2024) Adsorptive removal of bisphenol a by polyethylene meshes grafted with an amino group-containing monomer, 2-(dimethylamino)ethyl methacrylate. Physchem 4:431–446. https://doi.org/10.3390/physchem4040030
58. Yadav P, Warkar SG, Kumar A (2024) Development of graphene oxide-incorporated biopolymer-carboxymethyl tamarind kernel gum-based hydrogel as an effective adsorbent for the sequestration of dye pollutants. Polym Eng Sci 64:4816–4833. https://doi.org/10.1002/pen.26883
59. Xu D, Yang J, Lou T, Wang X (2024) Preparation of molecularly imprinted chitosan/ carboxymethyl cellulose Hollow vesicles for selective dye adsorption. Cellulose 31:4291–4303. https://doi.org/10.1007/s10570-024-05870-4
60. Yin H, Wang H, Wang D, Shi M, Xu X, Yang J (2024) NH_2-UiO-66 (Zr) modified waste wool fibers for efficient adsorption of dye from water. Desalin Water Treat 318:100305. https://doi.org/10.1016/j.dwt.2024.100305
61. Chauhan S, Kumar P, Chauhan S, Ranote S, Jamwal P, Kumar K (2025) Kinetic and thermodynamic evaluation of sulfonated Guar gum-based hydrogels for effective and rapid adsorption of cationic dyes. J Disper Sci Technol 46:244–262. https://doi.org/10.1080/01932691.2023.2288102
62. Huang B, Liu Y, Li B, Wang H, Zeng G (2019) Adsorption mechanism of polyethyleneimine modified magnetic core–shell Fe_3O_4@SiO_2 nanoparticles for anionic dye removal. RSC Adv 9:32462–32471. https://doi.org/10.1039/C9RA06299H
63. Huang X, Qiu C, Chen Y, Zhang X, Qi J, Jiang Y, Hoop CF, Huang X (2023) Nanocellulose–based polyurethane foam adsorbent for pressure–driven dye–contaminated water purification.

Environ Sci Poll Res 30:93817–93829. https://doi.org/10.1007/s11356-023-29098-0
64. Moulahoum H, Ghorbanizamani F (2025) Development of a Semi–IPN xerogel composite from eggshell, hydroxyapatite, and Chitosan for efficient dye removal in aqueous media. J Polym Res 32:111. https://doi.org/10.1007/s10965-025-04342-y
65. Safarzadeh H, Peighambardoust SJ, Hamed MS, Reza M, Hadi PS (2022) Adsorption of Methyl Violet dye from wastewater using poly(methacrylic acid–co–acrylamide)/bentonite nanocomposite hydrogels. J Polym Res 29:113. https://doi.org/10.1007/s10965-022-02956-0
66. Herab AA, Ostadrahimi DSA, Olad A (2022) Synthesis of innovative TiO_2–inulin–Fe_3O_4 nanocomposite for removal of Ni (II), cr (III), crystal Violet and malachite green from aqueous solutions. J Polym Res 29:321. https://doi.org/10.1007/s10965-022-03186-0
67. Kumar R, Sharma R, Singh AP (2019) Synthesis and characterization of cellulose based graft copolymers with binary vinyl monomers for efficient removal of cationic dyes and Pb(II) ions. J Polym Res 26:135. https://doi.org/10.1007/s10965-019-1790-9
68. Nakhjiri MT, Marandi GB, Kurdtabar M (2018) Effect of bis[2-(methacryloyloxy)ethyl] phosphate as a crosslinker on poly(AAm-co-AMPS)/Na-MMT hydrogel nanocomposite as potential adsorbent for dyes: kinetic, isotherm and thermodynamic study. J Polym Res 25:244. https://doi.org/10.1007/s10965-018-1625-0
69. Chen S, Guo H, Yang F, Di X (2016) Cyclodextrin-grafted thiacalix [4]arene Netty polymer based on the click chemistry: Preparation and efficient adsorption for organic dyes. J Polym Res 23:28. https://doi.org/10.1007/s10965-016-0920-x
70. Saberi A, Alipour E, Sadeghi M (2019) Superabsorbent magnetic Fe_3O_4-based starch-poly (acrylic acid) nanocomposite hydrogel for efficient removal of dyes and heavy metal ion from water. J Polym Res 26:271. https://doi.org/10.1007/s10965-019-1917-z
71. Zhang Y, Wang D, Bai X, Xu J, Zhang J, Zhang G, Huang C, Liu W, Huang C, Xiong X (2023) Microfluidic Preparation of magnetic Chitosan microsphere and its adsorption towards congo red. J Polym Res 30:77. https://doi.org/10.1007/s10965-022-03387-7
72. Wang H, Luo W, Guo, Li D, Xue B (2022) Effective adsorption of congo red dye by magnetic Chitosan prepared by solvent-free ball milling. Mater Chem Phys 292:126857. https://doi.org/10.1016/j.matchemphys.2022.126857
73. Fawzy MA, Gomaa M (2021) Low-cost biosorption of methylene blue and congo red from single and binary systems using *Sargassum latifolium* biorefinery waste/wastepaper xerogel: an optimization and modeling study. J Appl Phycol 33:675–691. https://doi.org/10.1007/s10811-020-02290-2
74. Thottathil S, Puttaiahgowda YM, Selvaraj R, Elambalassery JG, Vinayagam R, Varadavenkatesan T (2025) Experimental and DFT studies of congo red and AB 113 dyes removal by adsorption and disinfection using novel. J Mol Liq 429:127628. https://doi.org/10.1016/j.molliq.2025.127628

Publisher's note Springer Nature remains neutral with regard to jurisdictional claims in published maps and institutional affiliations.

Springer Nature or its licensor (e.g. a society or other partner) holds exclusive rights to this article under a publishing agreement with the author(s) or other rightsholder(s); author self-archiving of the accepted manuscript version of this article is solely governed by the terms of such publishing agreement and applicable law.